Korean J. Chem. Eng., 35(8), 1650-1661 (2018)
DOI: 10.1007/s11814-018-0066-0

pISSN: 0256-1115
eISSN: 1975-7220

Attapulgite/carbon composites as a recyclable adsorbent for antibiotics removal

Jie Tang*,, Li Zong*,***,†, Bin Mu*,***, Yuru Kang*,***, and Aiqin Wang*,***,†**

*Key Laboratory of Clay Mineral Applied Research of Gansu Province, Center of Eco-materials and Green Chemistry, Lanzhou Institute of Chemical Physics, Chinese Academy of Sciences, Lanzhou 730000, P. R. China
**University of Chinese Academy of Sciences, Beijing 100049, P. R. China
***Center of Xuyi Palygorskite Applied Technology, Lanzhou Institute of Chemical Physics, Chinese Academy of Sciences, Xuyi 211700, P. R. China
(*Received 20 February 2018 • accepted 19 April 2018*)

Abstract−We evaluated the adsorption performance of attapulgite/carbon (APT/C) composite as reusable adsorbents for antibiotics. APT/C composite was first synthesized by one-step calcination based on the spent bleaching earth after bleaching of vegetable oil, and followed by a thermal regeneration after adsorption of antibiotic at different temperatures. Antibiotics adsorption results revealed that APT/C composites prepared at 300 °C exhibited high adsorption capacity and fast equilibrium. Thermal regeneration proved to be an efficient methodology for recycling the spent antibiotic-loaded APT/C composites. After the ten-time continuous adsorption-calcination process, the removal ratios of the recycled adsorbents still retained around 67.3% and 62.9% for chlortetracycline and tetracycline, respectively. The conjugation of the adsorption and regeneration results suggested that combining the advantages of APT and carbon species provided a feasible strategy to fabricate a promising adsorbent with the desirable adsorption and regeneration properties for removal of antibiotics in the future.

Keywords: Attapulgite, Composite, Cyclic Regeneration, Adsorption, Antibiotic

INTRODUCTION

Carbon-based adsorbents are increasingly performing a major role in emerging environmental remediation technologies [1]. Compared with conventional adsorbents, they have led to new avenues for novel applications in water treatment due to high surface area, high chemical/thermal stability, ease of chemical or physical modification, adjustable properties for specialized applications, and exceptional capacity for removal of both organic and inorganic contaminants [2-4].

As a consequence, interest in carbon-based adsorbents and their respective composites has progressed amazingly and represents a very hot topic in the quest for new challenges. However, the use of carbon-based adsorbents could suffer from some difficulties in cost due to the elaboration of these materials with pure organic compounds as carbon precursors [5,6]. In addition, aggregation behavior of such materials will inevitably exist, associated with environmental undesirable regeneration operations, which severely limits their wide application in high-efficient environmental related fields [7]. Therefore, it is imperative to develop more sustainable types of carbon-based adsorbents for overcoming the above-mentioned issues.

Clay minerals have been proposed as adsorbent and show fascinating results in terms of environmental pollution control in relation to organic or inorganic pollutants removal [8]. Also, their abundance in nature, low cost, higher stability, nuisancelessness and available properties make them a good candidate for developing carbon-based adsorbents as the supporters [9]. Subsequently, a novel class of clay minerals/carbon composites fabricated by the assembly of clay minerals with diverse organic precursors are thus among the most promising candidates as alternatives to high-cost carbon-based adsorbents for wastewater treatment in recent decades [10,11]. Obviously, the impregnation of clay minerals into carbon-based adsorbents not only reduces the cost of such applications and exposes more available active sites aiming to extend their potential functionalities, but also improves the aggregate phenomenon to some extent.

Spent bleaching earth (SBE), obtained from the refining process of crude vegetable oil, is actually a waste by-product. In step with the worldwide consumption of more than 60 Mt of vegetable oil, about 600,000 t of SBE are generated worldwide in the oil refining industry [12]. Most of which are usually burned and discarded as garbage, used as feed additives or used as low-value filler [13]. Thus, SBE has led to offering many possibilities for the preparation of improved cost-effective carbon-based adsorbents due to the residual of organic matters to make the ecosystem more sustainable. Clay minerals/carbon composite derived from SBE can effectively remove a wide range of pollutants; however, the regeneration of the exhausted adsorbents has proven to be a complicated and time-consuming process with low desorption rate by conventional elution process (organic solvents or acidic/basic solutions), which results in the secondary pollution and the limited applications, as described in our previous study [14]. To the best of our knowledge, little information is available for the studies on the continuous cyclic utilization of

†To whom correspondence should be addressed.
E-mail: zongli@licp.cas.cn, aqwang@licp.cas.cn

the exhausted clay minerals/carbon composites for removal of pollutants.

Bearing this in mind, the aim of this study was to open a new avenue to explore sustainable attapulgite/carbon (APT/C) composites synthesized by carbonization of SBE for the chlortetracycline (CTC) and tetracycline (TC) removal, while also highlighting their continuous cyclic adsorption of antibiotics using the exhausted APT/C composites by thermal regeneration techniques. The physical-chemical properties of APT/C composites along with the influence of calcination temperature, initial pH, initial concentration of antibiotics, contact time and regeneration temperature were systematically investigated. The effect of successive regeneration cycles was also analyzed.

MATERIALS AND METHODS

1. Materials

Spent bleaching earth from soybean oil bleaching was marked as SBE consisting essentially of APT and approximately 21.8% organic matter (e.g., fatty acids, grease, etc.), and was supplied by Jinguang Food Co. LTD. (Zhejiang, China). Chlortetracycline (CTC) and tetracycline (TC) were USP grade purchased from Shanghai Aladdin Reagent Inc., China. The physical characteristics and molecular structure of CTC and TC were presented in Table S1. All other chemicals were of analytical grade and used as received without further purification.

2. Preparation of APT/C Composites

The APT/C composites were fabricated by one-step calcination method. Specifically, 30.0 g of the SBE was treated in the furnace by heating to five different temperatures (200, 300, 400, 500 and 600 °C) with a heating rate of 10 °C min^{-1}, and held at the final temperature for 2 h in air atmosphere, respectively. The resultant samples were labeled as APT/C-x, where x referred to the above calcination temperatures.

3. Evaluation of Adsorption Properties

Batch adsorption experiments were performed by mixing 20 mL of the CTC or TC solution (200 mg/L) with 20 mg as-prepared composite. The mixtures were shaken in a thermostatic orbital shaker (THZ-98A) at 25±5 °C/160 rpm for a certain time, and then the composite was divided from the solution by centrifugation. Subsequently, an appropriate amount of supernatant was sampled and diluted to the desired concentration of CTC and TC for determination using a UV-vis spectrophotometer at the wavelength of maximum absorbance of 397 and 392 nm, respectively. The adsorption capacity (Q_e, mg/g) and the removal efficiency (RE, %) toward CTC or TC were quantified by the differences in the concentration before and after the adsorption according to the following Eq. (1) and Eq. (2), respectively:

$$Q_e = \frac{(C_0 - C_e) \times V}{m} \quad (1)$$

$$RE(\%) = \frac{C_0 - C_e}{C_0} \times 100\% \quad (2)$$

where C_0 and C_e are the initial and equilibrium concentrations (mg/L), V is the volume of solution (mL) and m is the mass of adsorbents used (mg), respectively.

The variables affecting the adsorption performance were investigated systematically. The effect of pH values on the adsorption capacity was evaluated by adjusting the initial pH of CTC and TC solution from 2 to 10 with 1.0 mol/L HCl or NaOH. A series of CTC and TC solutions with the concentrations of 50-1,000 mg/L were contacted with 20 mg adsorbent for 4 h and natural pH to investigate the adsorption isotherms. The adsorption kinetics was performed by varying the adsorption time from 10 to 360 min and natural pH with three concentration levels (100 mg/L, 300 mg/L and 600 mg/L).

4. Thermal Regeneration of Spent APT/C Composites

To perform the thermal regeneration of spent APT/C composites, APT/C-300 after adsorption of CTC or TC was employed as the probe for investigation, respectively. In this process, regeneration temperature of the spent samples was implemented by a muffle furnace with air and calcined at various temperatures (200-800 °C) with a heating rate of 10 °C min^{-1} for 2 h to investigate the regeneration conditions. The adsorption experiments of the regenerated APT/C-300 were enforced by addition of 20 mg adsorbent in 20 mL 600 mg/L CTC or TC aqueous solution at 298 K for 6 h. The adsorption capacity of the regenerated APT/C-300 after each regeneration cycles was determined by the same procedure described above. For this study, ten consecutive thermal regeneration cycles were carried out.

5. Analytical Methods

Fourier transform infrared (FTIR) spectra were recorded on a Thermo Nicolet NEXUS TM spectrophotometer with incorporation of solid samples using KBr in wavelength range of 4,000-400 cm^{-1}. X-ray diffraction (XRD) patterns were detected using an X'Pert PRO diffractometer (X'Pert PRO, PAN analytical Co., NLD) using the Cu-Kα radiation in the range of 2θ=3-80° at 40 kV and 40 mA. The micrographs of the samples were taken using a field emission scanning electronic microscope (SEM, JSM-6701F, JEOL, Ltd. Japan) and a transmission electron microscopy (TEM, JEM-2010, JEOL, Tokyo, Japan). The elemental composition of the as-prepared samples was conducted by a Kevex energy dispersive spectrometer (JSM-5600LV, Japanese Electronic Optical Co., LTD., Japan). Thermogravimetric (TG) analysis was obtained from an STA 6000 (Perkin-Elmer Instrument Co., Ltd. USA) over a temperature interval of 30-800 °C at a rate of 10 °C min^{-1} in O_2 atmosphere. The Raman spectrum (Raman) was recorded on a Horiva (Lab Ram HR-800) spectrometer. Brunauer-Emmett-Teller (BET) surface area, pore size and pore volume were measured using an ASAP 2020 instrument (Micromeritics, USA). Zeta potentials of suspensions were measured on a Malvern Zetasizer Nano system with irradiation from a 633 nm He-Ne laser (ZEN3600, Britain). The absorbance of the samples was measured using a UV-vis 765 spectrophotometer (Precision & Scientific Instrument Co., Ltd., Shanghai, China).

RESULTS AND DISCUSSION

1. Structural Characterization of APT/C Composites

1-1. XRD and FTIR Analysis

Fig. 1(a) shows the XRD patterns of SBE and the various APT/C composites calcined at different temperatures. APT is the main com-

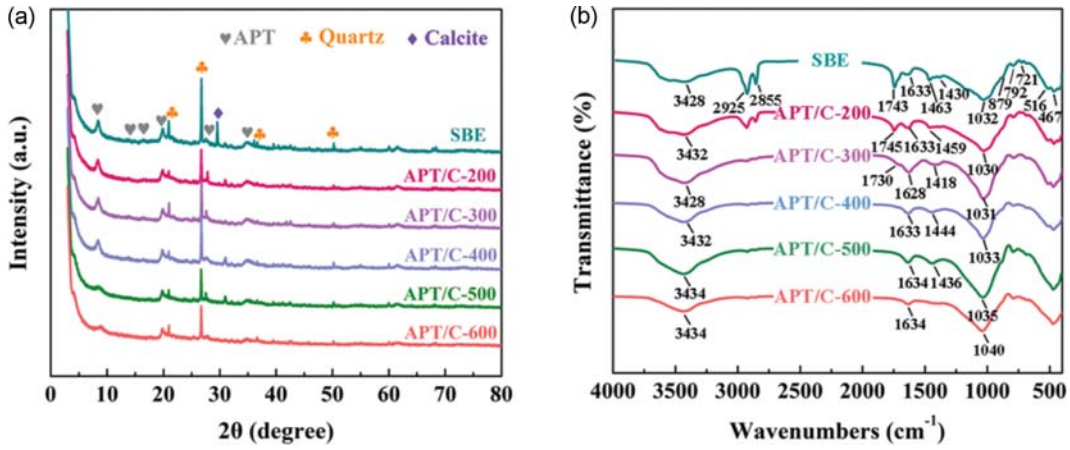

Fig. 1. (a) XRD patterns and (b) FTIR spectra of SBE and APT/C composites.

ponent phase in the SBE used in this study, with appreciable amounts of quartz and calcite coexisted in the samples. After calcination, the crystal structure is maintained perfectly differing only in terms of the intensity of the diffraction peaks of APT. Interestingly, the relative intensity of these diffraction peaks weakens evidently or almost vanishes after calcinated at 600 °C, especially 2θ=8.38°, indicating the deformation of layer-ribbon structure of APT and the damage of the ordered arrangement of lattice structure after calcination [15]. Furthermore, all the APT/C composites present broad diffraction peaks centered at 2θ of around 20° corresponding to the characteristic peak of carbon-based materials, implying the formation of carbonaceous materials after calcination of SBE at different temperatures [16]. The decrease in the intensity of this peak compared with that of the raw SBE may be attributed to the decomposition of carbon species.

The FTIR spectra of SBE and the as-prepared APT/C composites calcined at different temperatures (200, 300, 400, 500 and 600 °C) are illustrated in Fig. 1(b). The asymmetric (2,855 cm^{-1}) and symmetric stretching vibrations (2,925 cm^{-1}) of C-H are remarkably weakened or even disappeared after the calcination treatment, reflecting the successful transformation from the residual organic matters to carbon species [17]. Moreover, the absorption peaks at 3,428, 1,633, 1,032 and 516 cm^{-1} can be assigned to the stretching vibration of Mg (Al, Fe) O-H in the octahedral sheet, H-O-H bending vibration of water molecules, Si-O-Si stretching vibration and the deformation of tetrahedral sheet, respectively, which are the characteristic peaks of APT [18]. After being calcined, the intensities of these peaks weaken or disappear owing to the effectiveness of removing the water molecules in the tunnel of APT and breaking the Si-O-Si bonds to gain the interaction between adsorbents with adsorbates [19]. In addition, calcite is detected in the SBE by its characteristic peak at 1,430 cm^{-1}, and the asymmetrical stretching vibration and deformation vibration of carbonate anions are also obvious from emergence of peaks at 879 cm^{-1} and 721 cm^{-1} [20]. The significant change of intensities for these peaks further validates the decomposition of impurities or associated minerals at elevated temperature.

In particular, the unsaturated soybean oil in the SBE exhibiting peaks at 1,743 cm^{-1} (C=O stretching vibration) and 1,463 cm^{-1} (C=C stretching vibration) are noticeable, implying that the surfaces of the APT/C composites are rich in hydroxyl, carboxyl, and aromatic groups, which potentially contribute to the antibiotics binding process through adsorption. Note that the intensity of the two peaks becomes extremely weaker after being calcined at 200 and 300 °C, and then virtually disappears when the calcination temperature is up to 300 °C. An incidence of peak at 467 cm^{-1} reveals the C-C bending vibration. Meanwhile, the peak of about 1,633 cm^{-1} is also assigned to C-H (aromatic stretching vibration), suggesting the aromatic carbon in this resulting composite [21]. Thus, it may be speculated that the structural changes in APT/C composites by carbonization temperature determine their adsorption performances towards antibiotics.

1-2. SEM and TEM Analysis

Fig. 2(a)-(f) shows the SEM images of SBE and APT/C composites with different calcination temperatures. The SBE is observed to be brown and covered with organic matters (Fig. 2(a)). Compared with SBE, the as-prepared APT/C composites present the typical nanorod-shaped structure of APT with different morphology characteristics, and a great amount of the rod-like structure gradually increases with further raising the calcination temperature due to the decomposition and carbonization of the residual organics. Furthermore, the obvious change in color of the APT/C composites after calcination also indicates that the calcination temperature has an important influence on the feature and component of the obtained APT/C composites (Fig. 2(b)-(f)). The formation of as-prepared composite can be further confirmed by TEM images. As the case of APT/C-300, it can be found that APT/C composite consists of rod-like APT and carbon species, where carbon nanosheets are attached on the surface of the one-dimensional APT (Fig. 2(g)-(i)). The effective combination of the two materials is expected to enhance the adsorption of antibiotics.

1-3. Raman Analysis

The Raman spectroscopic data provides important information about the microcrystalline carbon structure of the materials. The Raman spectra of the APT/C composites obtained at different temperatures are analyzed in Fig. 3. Two noticeable peaks at around 1,365 cm^{-1} and 1,591 cm^{-1}, assigned to the D band and G band, respectively, are detected in all APT/C samples, suggesting similar

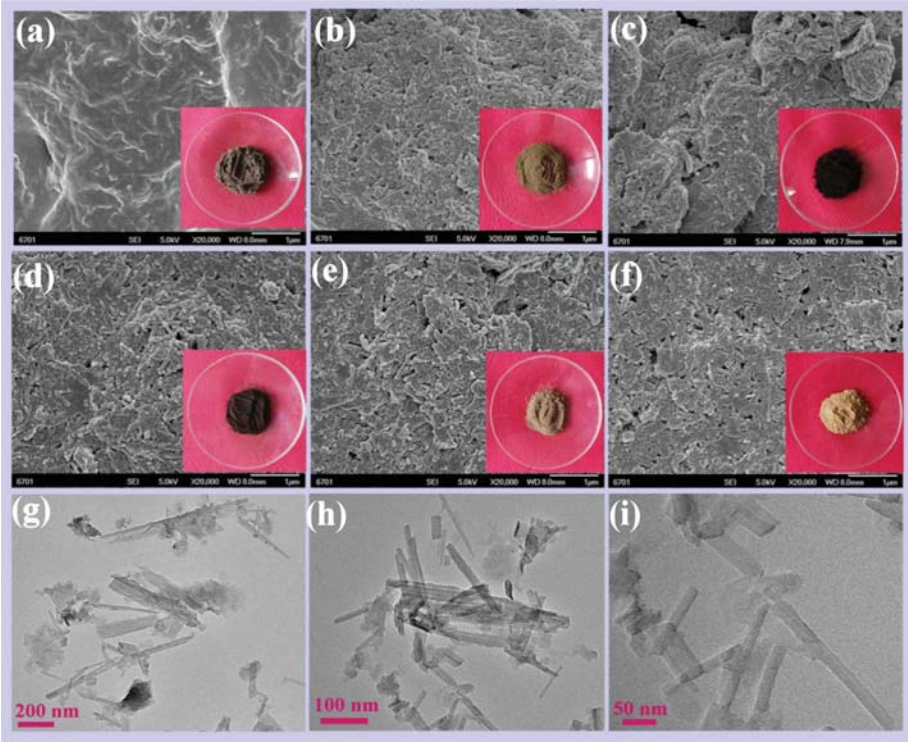

Fig. 2. SEM images and digital photographs of (a) SBE, (b) APT/C-200, (c) APT/C-300, (d) APT/C-400, (e) APT/C-500, (f) APT/C-600, and (g)-(i) TEM images of APT/C-300.

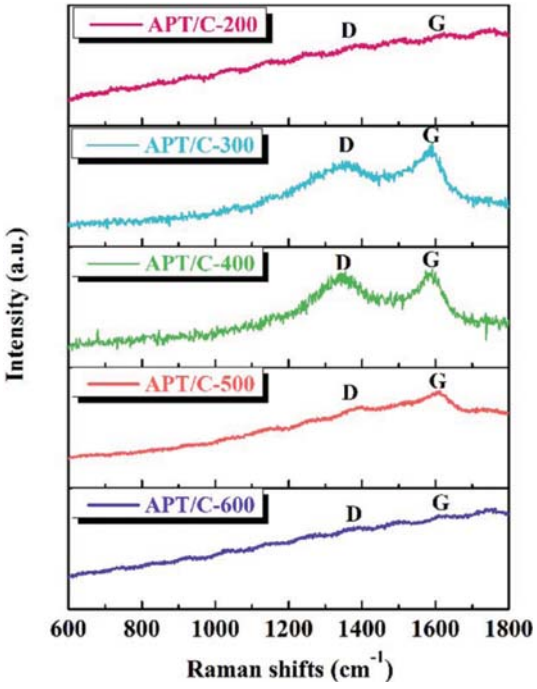

Fig. 3. Raman spectra of APT/C composites.

graphitelike crystallite and amorphous carbon structure of the samples. Concerning D and G bands, they originate from the defects and disorders existing in carbonaceous material and from E_{2g} in-plane bond stretching modes of pairs of sp^2 carbons, respectively [22]. Furthermore, it is widely accepted that the intensity ratio of those two peaks (I_D/I_G) is the extent of disorders or defects of the carbon structure [23]. During calcination treatment, band positions are approximately invariable, while their relative intensities and widths significantly change. As calculated, the I_D/I_G values of APT/C composites are 0.931 (200 °C), 0.855 (300 °C), 0.859 (400 °C), 0.922 (500 °C), and 0.929 (600 °C).

The higher the value of I_D/I_G, the lower the degree of graphitization of the APT/C composites [24,25]. The results confirm that the optimum calcination temperature is 300 °C for the production of APT/C composite with high degree of graphitization compared to the samples prepared at other temperatures. This phenomenon is distinct from common sense that a higher carbon graphitization degree could be obtained at high-temperature calcination. A similar trend can be discovered by the formulation of nitrogen-doped hierarchically porous carbon materials owing to the presence of more disordered carbon originating from the pores generated during the calcination process [26]. On the contrary, the APT/C composite, although heated up to 600 °C, only offers weaker broad bands at the corresponding positions, implying the deformation of APT associated with its amorphous nature with low graphitization, being in accordance with the XRD results.

1-4. TG and Pore Structural Parameters Analysis

TG analysis was performed to determine the actual carbon species loading in the APT/C composites (Fig. 4(a)). The main mass loss below 200 °C is almost the same for all samples, which is assigned to the removal of all surface-adsorbed water, zeolite water and partial coordinated water. While the weight loss in the temperature range of 200-600 °C may be mostly due to the decomposition of carbon

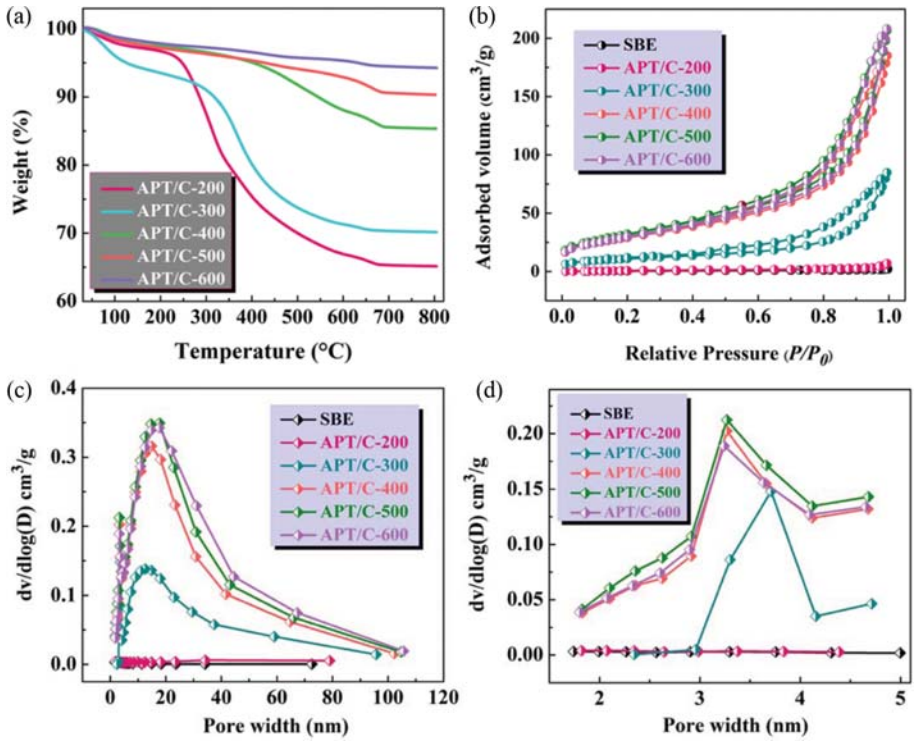

Fig. 4. (a) TG curves of APT/C composites, (b) N_2 adsorption/desorption isotherms, (c) BJH pore size distributions, and (d) BJH pore size distributions in the range of 1-5 nm of SBE and APT/C composites.

species under O_2 atmosphere. Compared with the TG curve of bare APT prepared at corresponding calcination temperatures, the total mass losses of APT, APT/C-200, APT/C-300, APT/C-400, APT/C-500 and APT/C-600 are 13.43%, 42.73%, 38.62%, 25.04%, 21.83% and 18.49%, respectively. Hence, the content of carbon species of APT/C-200, APT/C-300, APT/C-400, APT/C-500 and APT/C-600 is about 29.3%, 25.19%, 11.61%, 8.4% and 5.06%, respectively. It is obvious that the mass loss of APT/C composites reduces with the increasing calcination temperature, indicating that the carbon species content of composites gradually decreases. The result is consistent with the analysis of SEM images.

To further understand the relationship between vesicular structures of APT/C composites and antibiotics adsorption process, specific surface area and average pore size of SBE and the as-prepared APT/C composites were examined. Fig. 4(b) shows the N_2 adsorption-desorption isotherms of SBE and APT/C composites. Regarding SBE, it shows non-porous material characteristic, which is ascribed to the low specific surface area owing to the existence of organic residues [27]. In contrast, APT/C-200 exhibits a typical type I isotherm as stated by IUPAC classification, showing that it is a microporous material. With the increase in the calcination temperature, IV isotherms with a typical H3 type hysteresis can be observed in APT/C composites, revealing the creation of micropore structure and widening of micropores to mesopores (and/or macropores). In addition, from the shape and hysteresis of the isotherms, it is plausible to suggest that APT/C composites show a more extensive microporous structure with the elevated calcination temperature.

The textural properties (e.g., specific surface area, total pore volume and average pore diameter) of the adsorbents are also summarized in Table S2. The specific surface areas of the APT/C composites increase substantially compared with those determined for SBE, resulting in more sites for the adsorption of antibiotics. Specifically, the specific surface area and pore volume of APT/C composites begin to increase in the whole range of 200-500 °C with the elevated temperature, and after that slightly decrease when the calcination temperature is up to 600 °C. These results can be explained by the disintegration of the organic matter and the structural change of APT. Interestingly, the co-occurrence of micropore surface area and micropore volume at the calcination temperature of 300 °C is important for the application in wastewater treatment.

The pore size distributions of SBE and the developed samples are also measured and the results are given in Fig. 4(c). It is evident that microporosity and mesoporosity mainly exist in APT/C composites with broad pore size distribution. A more gradual increase in main pore diameter according to the peak can be observed during higher calcination treatment (Fig. 4(d)). As a whole, the pore size distributions widen and shift towards larger pores as the calcination temperatures increase, leading to larger average pore size, as listed in Table S2. These results overall validate that the total optimization of the pore characteristics is important for facilitating antibiotics adsorption.

1-5. EDS Analysis

Furthermore, EDS analysis was done to probe the presence of involved elements of SBE and APT/C-300, and their atomic percent with different elements is demonstrated in Fig. 5. It is apparent that the O, Fe, Al, Si, and Mg contained in SBE are typical of the elemental composition of APT [28]. Similar to raw clay, Si, O,

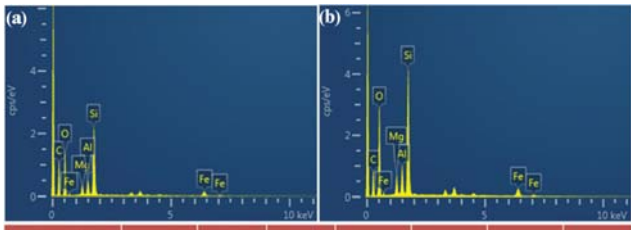

Atomic percent (%)	C	O	Si	Mg	Al	Fe	C/O
SBE	56.49	34.33	5.79	1.14	1.37	0.88	1.65
APT/C-300	42.02	44.07	8.72	1.82	2.11	1.26	0.95

Fig. 5. EDS spectra of (a) SBE and (b) APT/C-300.

Mg, Al, and Fe are the existing elements in APT/C-300. Notably, only the difference on the element contents between SBE and APT/C-300 can be observed. That is, the ratio of C/O is decreased from 1.65 to 0.95 after calcination. A significant decrease in C/O ratio on the APT surface can be related to the decomposition of retained organic matters and the generation of oxygen functional groups, confirming its role in adsorption of antibiotics by APT/C-300. All the informations provide evidence that APT/C composites have been successfully fabricated by calcination process, and the resulting APT/C composites will show a significant adsorption for antibiotics.

2. Optimization of the Calcination Conditions

To obtain a promising adsorbent with exceptional adsorption properties, the effect of calcination temperature on CTC and TC adsorption was evaluated. As illustrated in Fig. 6, the adsorption capacities of the APT/C adsorbent for CTC and TC initially increase with increasing the calcination temperature, reaching the maximum at temperature of 300 °C, followed by a slight decline with prolonging the calcination temperature, revealing that the production of excellent adsorbent is sensitively rely on the moderate temperature. At low calcination temperature (200 °C), the rod-like crystal structure of APT has no obvious change, and only a small portion of water molecules are removed from APT. With increasing calcination temperature to 300 °C, the removal of considerable amount of water results in the increase in specific surface area of the sample, and the APT/C composite is rich in functional groups (hydroxyl groups, carboxyl groups, etc.), in accord with the trends in the zeta potential (Fig. S1), contributing to the adsorption associated with the electrostatic attraction. Upon further increasing the calcination temperature to 600 °C, a decline in the adsorption capacity of APT/C composites is clearly observed. This trend can be due to the folding or complete collapsing of the APT skeleton and decomposing of carbon species caused by rising the calcination temperature. Comparatively, 300 °C is considered the optimal calcination temperature to develop an encouraging adsorbent with extraordinary performance.

3. Variables Influencing Adsorption Properties

3-1. pH

Fig. 7(a) presents the influence of initial pH on the adsorption of APT/C-300 for CTC and TC. The adsorption capacity of CTC increases with increasing pH and reaches a maximum value when the pH value is 4, whereas the adsorption capacity is gradually weakened to a certain extent when the pH value is further adjusted to above 7. The trend of the adsorption capacity for TC in the studied pH range is accordance with that for CTC. TC adsorption increases with the increase in initial pH and reaches small plateaus at pH range 4-7, and then starts to decrease from pH 8. Since the adsorption process occurring always includes electrostatic interaction, hydrogen bonding, electron donor-acceptor and π-π interaction involved in the studied pH range [29], such pH dependent phenomenon might be related to the surface charge of the adsorbent, the molecular structure of antibiotics, as well as the functional groups presenting on the surface of adsorbent.

Taking TC adsorption as an example, TC can exist in four forms of TCH_3^+ (pH<3.3), TCH_2^0 (3.3<pH<7.7), TCH^- (7.7<pH<9.7), and TC^{2-} (pH>9.7) at different pH levels [30]. In a fundamental sense, the protonated form of APT/C-300 is predominant at the lower pH, while TC exhibits the cationic species; thereby, the electrostatic repulsion between the adsorbent and adsorbate as well as the competition between H^+ and TCH_3^+ result in a lower adsorption capacity. Nevertheless, strong π-π interaction can occur between the π systems on APT/C-300 surface and benzene rings in TC molecules, probably achieving a considerable amount of TC adsorbed on APT/C-300 surfaces at pH 3.0 [31]. Subsequently, the adsorption capacity increases and the maximum adsorption capacity is achieved in the pH of 4.0. As the pH increases to 7.0, the dominant TC species is TCH_2^0, the adsorption capacity is stable due to the

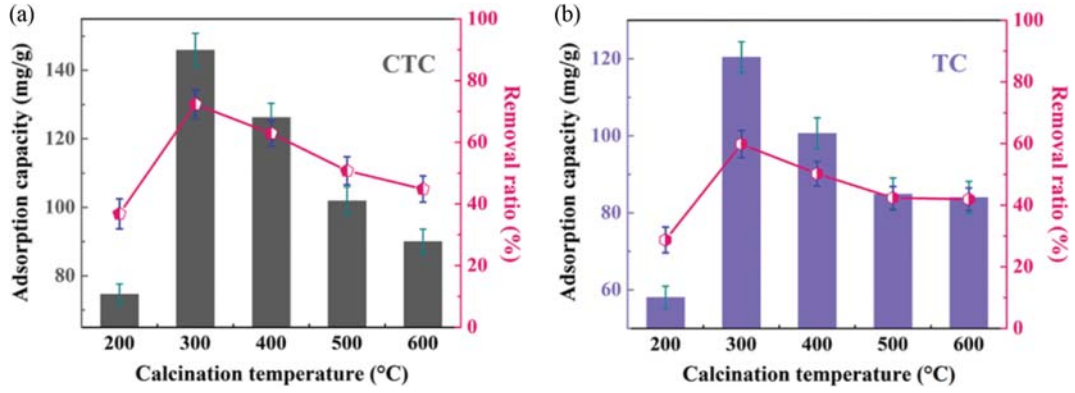

Fig. 6. Effect of calcination temperatures on the adsorption capacity of APT/C composites for (a) CTC and (b) TC.

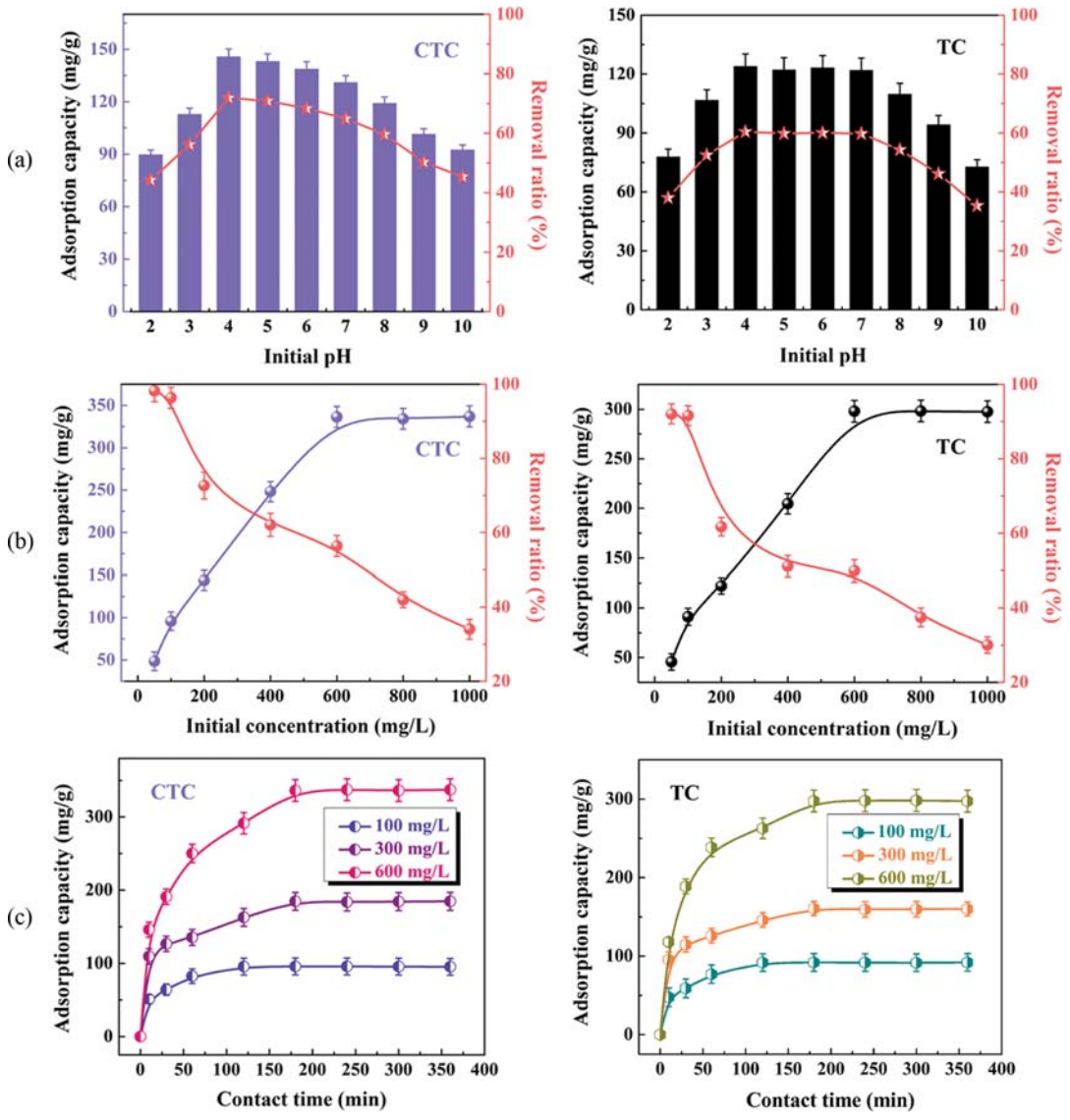

Fig. 7. Effect of (a) initial pH, (b) initial concentration and (c) contact time on the adsorption capacity of APT/C-300 for CTC and TC.

weak electrostatic interaction between TC and the deprotonation of adsorbent surface. At higher pH values, the dissociation of TC molecule transforms it to TCH^- and TC^{2-}; thus, the stronger electrostatic repulsion between the negatively charged adsorbent and the anionic character of TC might cause poor adsorption capacity. Consequently, in all the batch adsorption experiments, an optimum pH value of 4.26 and 3.68 is fixed for CTC and TC, respectively.

3-2. Initial Concentration of Pollutants

As shown in Fig. 7(b), the adsorption capacity of APT/C-300 for CTC and TC increases sharply with further increasing the initial concentration. This may be because the concentration of adsorbates provides the necessary driving force to surmount the resistance between the solution and the adsorbent surface [32]. However, the CTC and TC removal ratios of APT/C-300 decrease with the increasing initial CTC and TC concentration, which may be due to the low availability of binding sites to attach CTC or TC in the adsorbents. Thereafter, the increasing tendency of adsorption capacities becomes flat, and the maximum adsorption capacities for CTC and TC at the equilibrium concentration of 600 mg/L are 336.37 mg/g and 297.91 mg/g, respectively. The high adsorption capacities for CTC and TC are closely related to the abundant functional groups and the sufficient pore structure. As a whole, the above-mentioned results prove the successful application of the as synthesized APT/C-300 for effective removal of antibiotics.

To further explore the adsorption mechanism, two well-known adsorption isotherms of Langmuir (Eq. (S1)) and Freundlich isotherm (Eq. (S2)) are used to fit the experiment data (Fig. S2). The different isotherm parameters with corresponding R^2 values determined from linearized equations of two isotherms are presented in Table S3. The Langmuir isotherm displays better straight lines with higher R^2 values around 0.98 than that fitted with Freundlich model, revealing a mono-layer adsorption with interaction between adsorbed molecules onto the homogeneous surface [33,34].

Table 1 and Table 2 compare the maximum adsorption capaci-

Table 1. Summary of adsorption capacity of CTC by several adsorbents

Adsorbent	Feedstock	Technique used	Q_{max} (mg/g)	Reference
Graphene oxide functionalized magnetic particles	Amine-functionalized magnetic particles, Graphene oxide	Template-free method	42.6	[31]
Granular Merck activated carbon (0.60-1.00 mm)	Commercial granular activated carbon	-	309.9	[35]
Activated pinewood biochar	Pine white wood	Pyrolysis	208.3	[36]
Sludge-derived adsorbent	Sewage sludge	Pyrolysis	30	[37]
APT/C-300	Spent bleaching earth	Calcination	336.4	This work

Table 2. Summary of adsorption capacity of TC by several adsorbents

Adsorbent	Feedstock	Technique used	Q_{max} (mg/g)	Reference
Rice husk ash	Rice husk ash	-	8.37	[38]
Ferric-activated SBA	Ferric sulfate Dried sludge	Pyrolysis	40.8	[39]
CK.750.5	Tyre pyrolysis char (TPC)	Pyrolysis	316.6	[40]
Magnetic polystyrene EDTA microsphere (MPEM)	PS-EDTA microsphere resins	Solvothermal method	166	[41]
APT/C-300	Spent bleaching earth	Calcination	297.9	This work

ties (Q_{max}) for adsorption of CTC and TC on APT/C-300 adsorbent with other available adsorbents, respectively. It is clearly obvious that the adsorption capacity of CTC or TC on the APT/C-300 appears to be much higher than that of some tabulated adsorbents. Accordingly, our cost-effective and facile preparation and outstanding properties make APT/C-300 an applicable and promising candidate in water purification.

3-3. Contact Time

Adsorption kinetic models are essential to assess the rate-controlling of adsorption process as well as to provide significant information on the reaction mechanism [42]. For this purpose, the adsorption of CTC and TC on APT/C-300 by using three concentrations of antibiotics from low to high level as a function of contact time is studied. As illustrated in Fig. 7(c), the adsorption capacity increases sharply initially, and then slows and finally reaches equilibrium. According to this increasing trend, the equilibrium times are sensitively relied on the initial antibiotics concentration. For CTC and TC adsorption, the adsorption equilibrium can be achieved within about 2 h and 3 h for low-level concentration of 100 mg/L and middle- and high-level concentration of 300 mg/L and 600 mg/L, respectively. The adsorption behavior may be explained by the increase in the driving force of the concentration gradient with an increase of initial antibiotics concentration and the abundance of available active sites for the adsorption of antibiotic molecules at the initial stage. Subsequently, the lower adsorption rate at the latter stage may be because of progressive exhaustion of remaining reactive sites and possible repulsive force between adsorbed molecules and bulk phase. Note that the faster rate of antibiotics adsorption onto APT/C-300 surface is owing to better accessibility of its surface, which originates from its larger surface area, and the stronger electrostatic attraction between antibiotic molecules and the surface sites contained in the adsorbent.

Based on the kinetic data obtained from the experimentation, pseudo-first-order (Eq. (S3)) and pseudo-second-order kinetic (Eq. (S4)) models have been used to clarify the adsorption process, as shown in Fig. S3. The kinetic parameters of CTC and TC under different initial concentrations are calculated and are given in Table S4. The higher correlation coefficient values (R_2^2>0.995) and closer q_e values with experimental data validate that adsorption of antibiotic molecules on APT/C-300 can be well characterized by the pseudo-second-order kinetic model nearly representing the process for all the solution concentration. This also means that a strong chemical interaction between adsorbate and adsorbent is rate-controlling and the adsorption capacity is proportional to the number of active sites of APT/C-300 [43]. Moreover, compared to the estimated kinetic constants (k_2) of CTC or TC for the three concentrations, the initial adsorption rate at low concentration (100 mg/L) is greater than middle or high concentration (300 mg/L and 600 mg/L), implying that the initial adsorption rates are overwhelmingly dependent on the initial concentration.

4. Recycling of Adsorbent

The recyclability of adsorbent and the removal efficiency of pollutants were also essential considerations in selecting suitable adsorbent, controlling pollution, and protecting environment, as most pollutants were either toxic or precious raw materials. To investigate the recycling performance of APT/C-300, simple thermal regeneration experiments were carried out to recycle adsorbents and recover pollutants. As the most applicable regeneration method, it is imperative to select optimal parameters and operating conditions for exhausting APT/C-300. In this case, the effect of regeneration temperature on adsorption efficiency of spent adsorbent is displayed in Fig. 8(a). As observed, the removal ratios of CTC and TC increase with the increase in the regeneration temperature and approach its maximum at 300 °C, followed by the removal ratios begin to decline. This phenomenon can be explained from the following aspects.

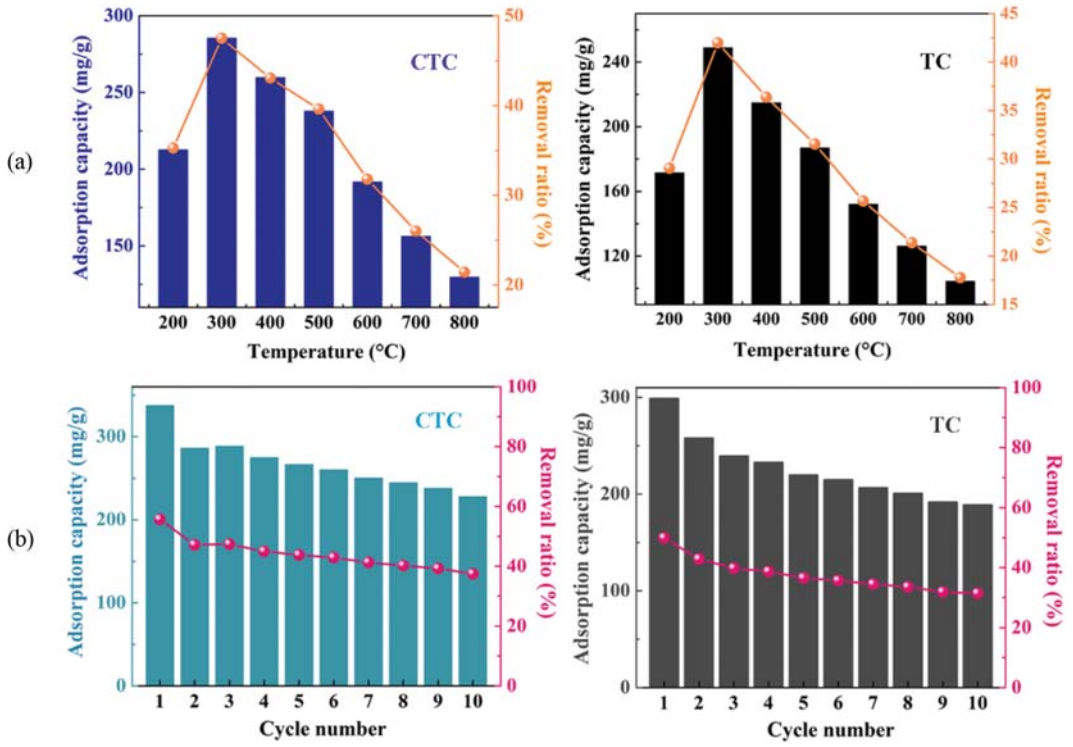

Fig. 8. (a) Effect of calcination temperatures on the adsorption capacity of CTC or TC-loaded APT/C-300 and (b) the amount adsorbed for CTC and TC as a function of adsorption-calcination cycle.

First, when the spent APT/C-300 is calcined at 200 °C after adsorption of antibiotics, the adsorbed antibiotics are not exhaustively eliminated, which is not conducive to the adsorption capacity in the next circle. At a high temperature of 300 °C, some oxidizing compounds are evolved from decomposing of the antibiotics adsorbed to the surface and pores of APT/C-300, such as CO and CO_2, thus releasing the increasing surface and pores for re-adsorption [44]. While the high temperature can prompt the decrease in intensity and size of pores due to deformation of nanotunnels of APT, leading to the reduction in the adsorption capacities for CTC and TC. In addition, the decrement of adsorption capacities may be responsible for the variation of surface functional groups and the decomposition of carbon species during regeneration at high temperature. In summary, 300 °C is the optimum calcination temperature for the thermal regeneration of the exhausted APT/C-300 after adsorption of antibiotics.

To certify the regeneration efficiency of the consumed APT/C-300 after being regenerated at 300 °C, the CTC and TC removal ratios of the regenerated APT/C-300 were also studied after ten adsorption-regeneration cycles (Fig. 8(b)). In terms of removal efficiency, 67.3% (CTC) and 62.9% (TC) of the initial adsorption capacity are still satisfactory in consideration of reducing disposal cost of the spent APT/C-300 after ten cycles for the regenerated adsorbent. With regards to the thermal degradation process itself, the adsorbent offers more and more resistance to the desorption of antibiotics after every cycle. This is related to the increasing permanence of strongly adsorbed compounds on the carbon surface, which resulted in a slight decay of the regeneration efficiency [45]. In the case of APT/C-300, the fraction of antibiotics removed is associated to the weaker bonds, while the fraction that remained adsorbed on the APT/C-300 surface is related to the chemisorbed species. Furthermore, partial small organic molecules emerging from the decomposition of antibiotics are attached to the surface of the regenerated APT/C-300. In particular, the oxygen-containing functional groups or carbon species primitively existing in the APT surfaces could either be partially removed or decomposed during the regeneration process. The above-mentioned reasons can be mainly responsible for the reduced adsorption capacity for antibiotics of the regenerated APT/C-300. As a whole, the APT/C-300 regenerated at optimized condition represents a fairly good stability to effectively treat the antibiotics, implying that the exhausted APT/C-300 can be reused in an eco-friendly way without much loss in adsorption capacity after proper thermal regeneration.

5. Proposed Mechanism of Antibiotics Adsorption

The FTIR spectra of APT/C-300, CTC and CTC-loaded APT/C-300 were performed and studied to gain an insight into the adsorption mechanism, as shown in Fig. 9(a). The characteristic adsorption peaks of APT/C-300 at 3,428 cm^{-1} (stretching vibration of O-H), 1,730 cm^{-1} (stretching vibration of C=O), 1,628 cm^{-1} (stretching vibration of aromatic ring and bending vibration of O-H), 1,463 cm^{-1} (stretching vibration of C=C) and 467 cm^{-1} (bending vibration of C-C) suggest the presence of many oxygen-containing functional groups and aromatic rings on APT/C-300. After the adsorption of CTC onto APT/C-300, the FTIR spectrum of CTC-loaded APT/C-300 exhibit many changes. The band at 3,428 cm^{-1} presented on APT/C-300 shifts to lower wavenumber (3,414 cm^{-1}), indicating O-H plays an important role in the adsorption process. Furthermore, the peak of APT/C-300 at 1,628 cm^{-1} that is assigned

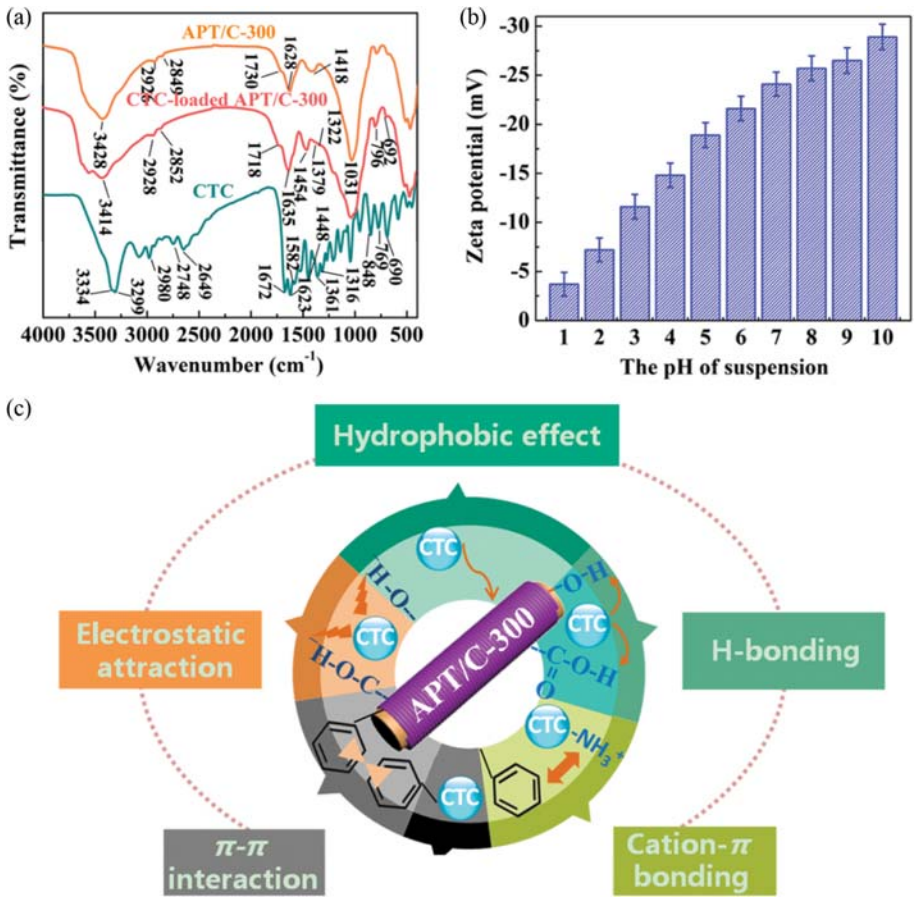

Fig. 9. (a) FTIR spectra of APT/C-300 before and after CTC adsorption, (b) zeta potentials of APT/C-300 in the pH range of 1-10, and (c) the feasible adsorption mechanism between APT/C-300 and CTC.

to aromatic ring shifts to 1,635 cm^{-1} after CTC adsorption; The C-H stretching vibration band of -CH_3 groups at 2,926 and 2,849 cm^{-1} shifts to 2,928 and 2,852 cm^{-1}, respectively; For CTC, the characteristic band of amide I at 1,623 cm^{-1}, amide II at 1,582 cm^{-1} shift to 1,635 cm^{-1} and overlap with the aromatic ring stretching vibration and O-H bending vibration of APT/C-300 at 1,628 cm^{-1}; Moreover, the C-N stretching band of benzene ring at 1,361 cm^{-1} and the amide III band at 1,316 cm^{-1} shift to 1,379 cm^{-1} and 1,322 cm^{-1}, respectively; The characteristic band of aromatic ring at 1,448 cm^{-1} still appears in the spectrum of CTC-loaded APT/C-300 (the band at 1,454 cm^{-1}); The -NH_2 bending vibration band of CTC at 848 cm^{-1} shifts to 796 cm^{-1} after adsorption.

These changes can be attributed to the following reasons. (i) The negatively charged surfaces of APT/C-300 resulting from the existence of numerous oxygen-containing functional groups can provide adsorption sites for electrostatic interaction with CTC and hydrophobic effect. In addition, the zeta potentials of APT/C-300 at different pH values of the suspension (Fig. 9(b)) confirm that the change in the adsorption capacity is consistent with the change in the negative zeta potential, which implies that the electrostatic attraction plays a positive role in enhancing adsorption; (ii) The π-π electron donor-acceptor interaction as a dominant driving force has been widely used to explain the adsorption of organic contaminants with benzene rings on the carbon surface [46]. The conjugated enone structures on CTC molecules act as π-electron-acceptors due to the strong electron-withdrawing ability of the ketone group. The -OH groups on the APT surface can make APT act as π-electron-donors. Therefore, strongly enhanced adsorption of CTC on APT/C-300 is expected via the formation of the stacking interactions [47]; (iii) Functional groups of CTC such as carbonyl and protonated amino could form hydrogen bond with oxygen-containing functional groups on APT/C-300; (iv) The cation-π bonding is dominated by the cation-induced polarization and electrostatic force between the cation and the permanent quadrupole of the π-electron-rich aromatic structure. Hence, the cation-π bonding between the protonated amino group on the ring C of CTC and the π-electrons in APT/C-300 might be another reasonable mechanism for adsorption. Moreover, the properties of nanometer scale, one-dimensional rod-liked morphology and relatively high specific surface area can make APT/C-300 contact and adsorb antibiotic molecules efficiently [48]. These aspects synergistically contribute to the high adsorption capacity and removal efficiency of APT/C-300 for antibiotics. The possible adsorption mechanism is schematically illustrated in Fig. 9(c).

CONCLUSION

This work shed light on the preparation and utilization of SBE-

derived APT/C composites as reusable adsorbents for antibiotics removal. The carbon species and functional groups on the APT surface endowed them with more active sites, hence facilitating the adsorption capacity and achieving the utilization of waste. It indicated that calcination temperature played a dominant role in antibiotics adsorption. The optimum temperature for the preparation of SBE-derived APT/C composites was 300 °C, where the maximum adsorption capacity of 336.37 mg/g for CTC and 297.91 mg/g for TC was obtained, respectively. In addition, the adsorption of as-prepared adsorbent for antibiotics had a pH-dependent and fast-responsive adsorption rate. More importantly, the exhausted APT/C-300 can be recycled by thermal regeneration at 300 °C in air with slight performance abasement after at least ten-times cycle. It was anticipated that APT/C composites can be produced economically and thermal regeneration for antibiotic-containing wastewater treatment.

ACKNOWLEDGEMENT

This work was supported by the National Natural Science Foundation of China (41601303), The funds for Creative Research Groups of Gansu, China (17JR5RA306) and Social Development Project of Science and Technology Plan of Jiangsu Province (BE 2017686) provided the financial support for this research.

SUPPORTING INFORMATION

Additional information as noted in the text. This information is available via the Internet at http://www.springer.com/chemistry/journal/11814.

REFERENCES

1. X. X. Jiang and D. K. Shen, *Korean J. Chem. Eng.*, **34**, 2619 (2017).
2. S. Y. Sawant, R. R. Pawar, S. M. Lee and M. H. Cho, *J. Clean. Prod.*, **168**, 290 (2017).
3. S. Q. Li, X. D. Zhang and Y. M. Huang, *J. Hazard. Mater.*, **321**, 711 (2017).
4. S. Shi, Y. W. Fan and Y. M. Huang, *Ind. Eng. Chem. Res.*, **52**, 2604 (2013).
5. S. Álvarez-Torrellas, R. S. Ribeiro, H. T. Gomes, G. Ovejero and J. García, *Chem. Eng. J.*, **296**, 277 (2016).
6. F. Q. An, D. Zhang, X. X. Yue, G. L. Ou, J. F. Gao and T. P. Hu, *Korean J. Chem. Eng.*, **33**, 576 (2016).
7. S. J. Zhang, T. Shao, H. Selcen Kose and T. Karanfil, *Environ. Sci. Technol.*, **44**, 6377 (2010).
8. P. S. Thue, A. C. Sophia, E. C. Lima, A. G. N. Wamba, W. S. De Alencar, G. S. Dos Reis, F. S. Rodembusch and S. L. P. Dias, *J. Clean. Prod.*, **171**, 30 (2018).
9. X. P. Wu, Q. X. Zhang, C. Li, X. L. Zhang and D. D. L. Chung, *Carbon*, **123**, 259 (2017).
10. X. Y. Liang, Y. Lu, Z. J. Li, C. Yang, C. Niu and X. T. Su, *Micropor. Mesopor. Mater.*, **241**, 107 (2017).
11. A. A. Alhwaige, H. Ishida and S. Qutubuddin, *ACS Sustainable Chem. Eng.*, **4**, 1286 (2016).
12. W. A. Oladosu, Z. A. Manan and S. R. Wan Alwi, *Chem. Eng. T.*, **56**, 133 (2017).
13. R. P. Singh, A. Embrandiri, M. H. Ibrahima and N. Esa, *Resour. Conserv. Rec.*, **55**, 423 (2011).
14. J. Tang, B. Mu, L. Zong and A. Q. Wang, *J. Clean. Prod.*, **172**, 673 (2018).
15. Z. F. Zhang, W. B. Wang and A. Q. Wang, *J. Environ. Sci.*, **33**, 106 (2015).
16. Y. Fan, R. F. Yang, Z. M. Lei, N. Liu, J. L. Lv, S. R. Zhai, B. Zhai and L. Wang, *Korean J. Chem. Eng.*, **33**, 1416 (2016).
17. M. Mana, M. S. Ouali and L. C. De Menorval, *J. Colloid Interface Sci.*, **307**, 9 (2007).
18. M. Suárez and E. Garcia-Romero, *Appl. Clay Sci.*, **31**, 154 (2006).
19. Z. F. Zhang, W. B. Wang, Y. R. Kang, L. Zong and A. Q. Wang, *Appl. Clay Sci.*, **120**, 28 (2016).
20. F. B. Reig, J. V. G. Adelantado and M. C. M. M. Moreno, *Talanta*, **58**, 811 (2002).
21. W. T. Tsai, H. P. Chen, M. F. Hsieh, H. F. Sun and S. F. Chien, *J. Anal. Appl. Pyrol.*, **63**, 157 (2002).
22. D. H. Yeom, J. Choi, W. J. Byun and J. K. Lee, *Korean J. Chem. Eng.*, **33**, 3029 (2016).
23. L. N. Wang, X. L. Jia, Y. F. Li, F. Yang, L. Q. Zhang, L. P. Liu, X. Ren and H. T. Yang, *J. Mater. Chem. A*, **2**, 14940 (2014).
24. C. Hu, S. Sedghi, A. Silvestre-Albero, G. G. Andersson, A. Sharma, P. Pendleton, F. Rodríguez-Reinoso, K. Kaneko and M. J. Biggs, *Carbon*, **85**, 147 (2015).
25. F. C. Tai, C. Wei, S. H. Chang and W. S. Chen, *J. Raman Spectrosc.*, **41**, 933 (2010).
26. X. Deng, B. Zhao, L. Zhu and Z. P. Shao, *Carbon*, **93**, 48 (2015).
27. M. Mana, M. S. Ouali, M. Lindheimer and L. C. De Menorval, *J. Hazard. Mater.*, **159**, 358 (2008).
28. W. F. Bradley, *Am. Mineral.*, **25**, 405 (1940).
29. D. Y. Zhang, J. Yin, J. Q. Zhao, H. Zhu and C. Y. Wang, *J. Environ. Chem. Eng.*, **3**, 1504 (2015).
30. B. Y. Huang, Y. G. Liu, B. Li, S. B. Liu, G. M. Zeng, Z. W. Zeng, X. H. Wang, Q. M. Ning, B. H. Zheng and C. P. Yang, *Carbohyd. Polym.*, **157**, 576 (2017).
31. Y. X. Lin, S. Xu and J. Li, *Chem. Eng. J.*, **225**, 679 (2013).
32. V. C. Srivastava, I. D. Mall and I. M. Mishra, *J. Hazard. Mater.*, **134**, 257 (2006).
33. P. N. Diagboya and E. D. Dikio, *J. Clean. Prod.*, **180**, 71 (2018).
34. X. P. Wu, Q. X. Zhang, C. Liu, X. L. Zhang and D. D. L. Chung, *Carbon*, **123**, 259 (2017).
35. R. Ocampo-Pérez, R. Leyva-Ramos, J. Rivera-Utrilla, J. V. Flores-Cano and M. Sánchez-Polo, *Chem. Eng. Res. Des.*, **104**, 579 (2015).
36. M. Taheran, M. Naghdi, S. K. Brar, E. J. Knystautas, M. Verma, A. A. Ramirez, R. Y. Surampalli and J. R. Valero, *Sci. Total Environ.*, **571**, 772 (2016).
37. R. Ding, P. F. Zhang, M. Seredych and T. J. Bandosz, *Water Res.*, **46**, 4081 (2012).
38. Y. J. Chen, F. H. Wang, L. C. Duan, H. Yang and J. Gao, *J. Mol. Liq.*, **222**, 487 (2016).
39. X. Yang, G. R. Xu, H. R. Yu and Z. Zhang, *Bioresour. Technol.*, **211**, 566 (2016).
40. R. Acosta, V. Fierro, A. M. De Yuso, D. Nabarlatz and A. Celzard, *Chemosphere*, **149**, 168 (2016).
41. B. Li, J. J. Ma, L. C. Zhou and Y. Qiu, *Chem. Eng. J.*, **330**, 191

(2017).
42. T. A. Saleh, A. Sarı and M. Tuzen, *Chem. Eng. J.*, **307**, 230 (2017).
43. B. D. Caprariis, P. D. Filippis, A. D. Hernandez, E. Petruccia, A. Petrullo, M. Scarsella and M. Turchi, *J. Environ. Manage.*, **197**, 231 (2017).
44. S. Román, B. Ledesma, J. F. González, A. Al-Kassir, G. Engo and A. Álvarez-Murillo, *J. Anal. Appl. Pyrolysis*, **103**, 201 (2013).
45. B. Ledesma, S. Román, A. Álvarez-Murillo, E. Sabio and J. F. González, *J. Anal. Appl. Pyrolysis*, **106**, 112 (2014).
46. F. Yu, J. Ma and D. S. Bi, *Environ. Sci. Pollut. Res.*, **22**, 4715 (2015).
47. Z. Q. Li, M. Y. Qi, C. Y. Tu, W. P. Wang, J. R. Chen and A. J. Wang, *Appl. Surf. Sci.*, **425**, 765 (2017).
48. J. W. Fu, Z. H. Chen, M. H. Wang, S. J. Liu, J. H. Zhang, J. N. Zhang, R. P. Han and Q. Xu, *Chem. Eng. J.*, **259**, 53 (2015).

Supporting Information

Attapulgite/carbon composites as a recyclable adsorbent for antibiotics removal

Jie Tang*,, Li Zong*,***,†, Bin Mu*,***, Yuru Kang*,***, and Aiqin Wang*,***,†**

*Key Laboratory of Clay Mineral Applied Research of Gansu Province, Center of Eco-materials and Green Chemistry, Lanzhou Institute of Chemical Physics, Chinese Academy of Sciences, Lanzhou 730000, P. R. China
**University of Chinese Academy of Sciences, Beijing 100049, P. R. China
***Center of Xuyi Palygorskite Applied Technology, Lanzhou Institute of Chemical Physics, Chinese Academy of Sciences, Xuyi 211700, P. R. China
(*Received 20 February 2018 • accepted 19 April 2018*)

SECTION I: SUPPLEMENTARY EXPERIMENTS

1. Adsorption Isotherms

The adsorption isotherms are fitted with two typical theoretical models: Langmuir model (Eq. (S1)) and Freundlich model (Eq. (S2)).

$$\frac{C_e}{q_e}=\frac{C_e}{Q_m}+\frac{1}{Q_m\times K_L} \quad (S1)$$

$$\log q_e=\log K_F+\frac{1}{n}\times\log C_e \quad (S2)$$

where C_e (mg/L) denotes the equilibrium concentration, Q_m and q_e (mg/g) are the adsorption capacity at equilibrium and at any time, K_L (L/mg) is the Langmuir constant related to the binding sites affinity, K_F ($mg^{(1-n)}L^n/g$) is the Freundlich constant and n represents the degree of sorption dependence at equilibrium concentration.

2. Adsorption Kinetics

In order to study the dynamic adsorption behaviors, the adsorption kinetic data are fitted using the pseudo-first-order (Eq. (S3)) and pseudo-second-order (Eq. (S4)) kinetic models.

$$\log(q_e-q_t)=\log q_e-\left(\frac{k_1}{2.303}\right)t \quad (S3)$$

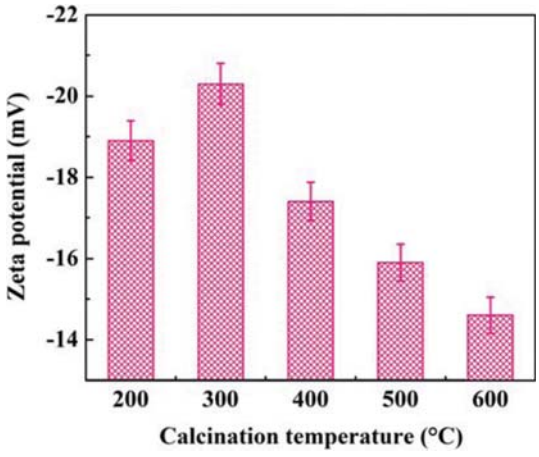

Fig. S1. The zeta potentials of APT/C composites at different calcination temperatures.

Table S1. The physical characteristics and molecular structure of CTC and TC

Compound	Chlortetracycline	Tetracycline
Abbreviation	CTC	TC
Chemical formula	$C_{22}H_{23}ClN_2O_8$	$C_{22}H_{24}N_2O_8$
Molecular weight (g/mol)	478.88	444.44
λ_{max} (nm)	397	392
Molecular structure	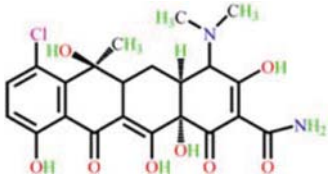	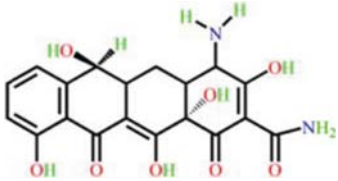
Ball-stick model	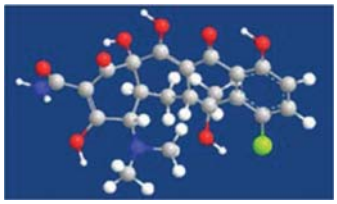	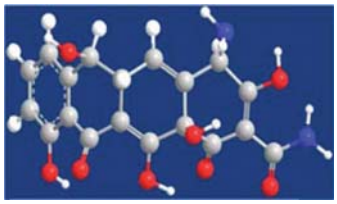

$$\frac{t}{q_t} = \frac{1}{k_2 q_e^2} + \frac{t}{q_e} \quad \text{(S4)}$$

where q_e (mg/g) and q_t (mg/g) are the adsorption amount of TC or CTC at equilibrium and time t (min), respectively. k_1 (min^{-1}) and k_2 ((g/mg)/min) are the rate constants of pseudo-first-order and pseudo-second-order model, respectively. The values of k_1 and k_2 can be calculated by the intercept and slope of the straight lines of $\log(q_e - q_t)$ vs t and t/q_t vs t, respectively.

SECTION II: SUPPLEMENTARY FIGURES AND TABLES

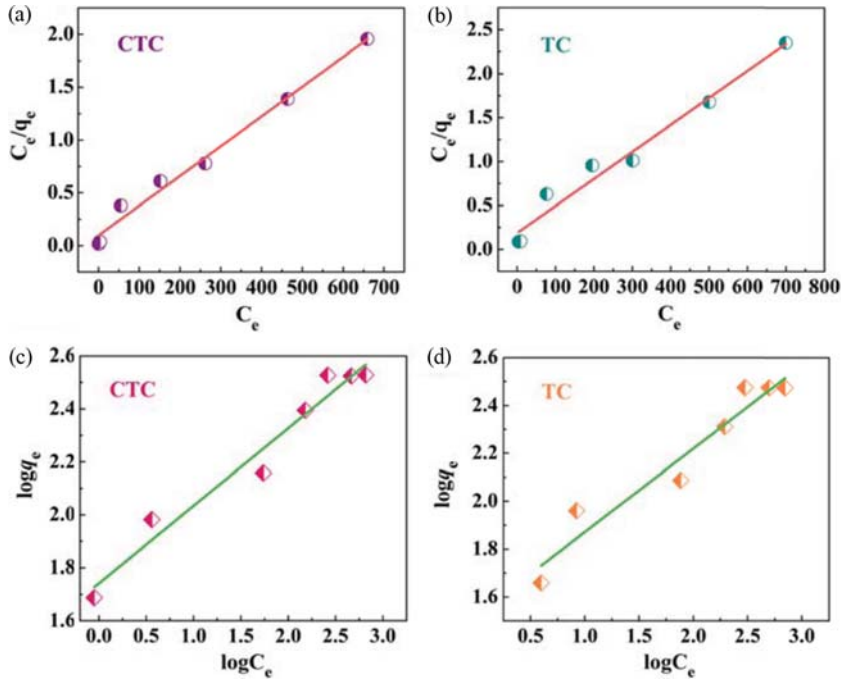

Fig. S2. Langmuir adsorption isotherms of (a) CTC and (b) TC on APT/C-300, and Freundlich adsorption isotherms of (c) CTC and (d) TC on APT/C-300.

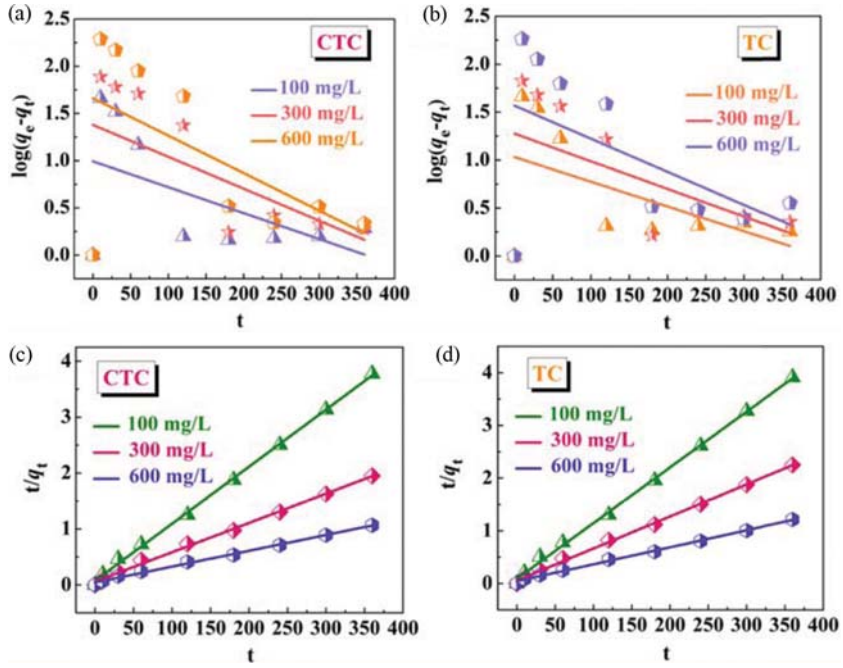

Fig. S3. Adsorption kinetic curves of (a) CTC, (b) TC on APT/C-300 by pseudo first-order kinetic model and (c) CTC, (d) TC on APT/C-300 by pseudo second-order kinetic model.

Table S2. The textural properties of SBE and APT/C composites

Sample	S_{BET} [a] (m^2/g)	S_{mic} [b] (m^2/g)	S_{ext} [c] (m^2/g)	V_{tot} [d] (cm^3/g)	V_{mic} [e] (cm^3/g)	D_{pore} [f] (nm)
SBE	2.8	-	4.1	0.0025		3.55
APT/C-200	7.6	0.6	6.9	0.0065	-	3.42
APT/C-300	39.5	3.7	35.8	0.1058	0.0012	10.71
APT/C-400	105.6	-	106.2	0.2499	-	9.47
APT/C-500	115.9	-	120.5	0.2762	-	9.54
APT/C-600	108.7	-	115.2	0.2718	-	10.01

[a]BET (Brunauer-Emmett-Teller) surface area
[b]Micropore surface area, derived from a t-plot method
[c]External surface area, calculated using a t-plot method
[d]Total pore volume, measured at P/P_0=0.97
[e]Micropore volume, obtained from a t-plot method
[f]Average pore diameter, calculated from D_{pore}=4 V/A according to BET

Table S3. Estimated isotherm parameters for adsorption of CTC and TC onto APT/C-300

Adsorbents	Adsorbates	Langmuir model				Freundlich model		
		$q_{e,exp}$ (mg/g)	$q_{e,cal}$ (mg/g)	K_L (L/mg)	R_L^2	K_F	n	R_F^2
APT/C-300	CTC	336.4	357.1	0.0291	0.9873	55.08	3.41	0.5810
	TC	297.9	322.6	0.0166	0.9731	33.28	2.87	0.9391

Table S4. Estimated adsorption kinetic parameters for the adsorption of CTC and TC onto APT/C-300

Adsorbents	Adsorbate	C_0 (mg/L)	$q_{e,exp}$ (mg/g)	Pseudo-first-order model			Pseudo-second-order model		
				$q_{e,cal}$ (mg/g)	k_1 (min^{-1})	R_1^2	$q_{e,cal}$ (mg/g)	$k_2\times10^4$ ((g/mg)/min)	R_2^2
APT/C-300	CTC	100	95.68	21.89	0.0094	0.6521	98.04	13.73	0.9987
		300	184.83	72.64	0.0122	0.8372	192.31	4.41	0.9968
		600	336.41	175.19	0.0145	0.8642	357.14	1.74	0.9959
	TC	100	91.83	24.65	0.0092	0.6947	94.34	12.23	0.9983
		300	160.74	52.65	0.0106	0.8042	163.93	6.53	0.9982
		600	297.87	130.86	0.0129	0.8396	312.50	2.37	0.9974